Advances in Concrete Construction, *Vol. 19*, *No. 1* (*2025*) *31-42*
https://doi.org/10.12989/acc.2025.19.1.031

Mechanical behavior of corrugated grouted sleeve splice for precast concrete structures under cyclic loading

Muwang Wei [1,2], Yukang Peng [1], Huawei Li*[1,2] and Boren Xiao [1]

[1] *School of Civil Engineering and Architecture, Wuyi University, 385 Baihua road, Wuyishang, Peoples' Republic of China*
[2] *Engineering Research Center of Prevention and Control of Geological Disasters in Northern Fujian, Fujian Province Higher Education Institutes, 385 Baihua road, Wuyishang, Peoples' Republic of China*

(*Received August 30, 2023, Revised December 27, 2024, Accepted January 3 2025*)

Abstract. To improve the splicing behavior of steel rebars in precast structures, this paper presents a novel corrugated grouted sleeve (CGS) fabricated at low cost from a rolling seamless pipe. To investigate the connection characteristics of splicing rebars in prefabricated structures under lateral loads, 18 specimens of 45# seamless pipe with various parameters were prepared and tested under cyclic loading. In general, the proposed connector system achieved high performance of the splicing rebars between precast components, ensuring sufficient integrity of the precast construction. Because the corrugated configuration provides sufficient anchoring strength for the steel rebars, the typical failure modes of the specimens under cyclic loading were steel rebar fractures, as desired. Moreover, cracks in the mortar were almost absent except at the ends, confirming higher performance than traditional sleeves. Finally, a method is proposed for capturing the confinement stress in the CGS for splicing steel rebars. The model results generally agreed with the test results. Therefore, it is believed that the proposed CGS system can be a alternative for splicing rebars in the prefabricated constructions.

Keywords: connection behavior; corrugation grouted sleeve; cyclic loads; precast structures

1. Introduction

In the past few decades, prefabricated constructions have been expected to reduce carbon emissions, conserve energy and resources, and realize green buildings (Elliott 2017, Kurama *et al*. 2018, Kuang and Zheng 2018, Lei *et al*. 2023). The connections between precast concrete elements are essential for ensuring sufficient stiffness and bearing capacity of the prefabricated structure under applied loading (Lee *et al*. 2013, Lu *et al*. 2019, Hemamalini and Vidjeapriya 2020, He *et al*. 2024). As the tensile strength of concrete is usually small and always ignored in the design procedure, the continuity and integrity of precast concrete constructions largely depend on their splicing steel rebars. In the early days, the reinforcement-bar splicing that delivers the force among the precast components was performed by three main methods: overlapping of the reinforcement bars, welding connections, and mechanical connections (Haber *et al*. 2014, Parastesh *et al*. 2014, Xiao *et al*. 2020, Sharbatdar *et al*. 2018, Kalogeropoulos *et al*. 2019, ACI 1999, Joshi *et al*. 2020). However, owing to various shortcomings, these methods are ineffective for splicing the steel rebars between precast concrete elements. Steel-bar lapping usually causes rebar congestion and requires a long overlapping length, whereas field welding is commonly difficult to apply and of uncertain quality. Mechanical connection usually requires a high installation accuracy (Ling *et al*. 2016, Alias *et al*. 2014, Henin and Morcous 2015, Al-Azzawi *et al*. 2020).

To overcome these challenges, Yee (Einea *et al*. 1995) proposed the grouted sleeve splice, in which the cement-based bonding material is injected into a metal sleeve. The loading applied on the steel bars is then transferred to the sleeve. New connection technology usually requires a short embedded length of the steel bars. Moreover, grouted sleeves are quickly and easily manufactured with low resource consumption, little noise, and minimal dust pollution. In tensile tests under uniaxial loading (Ameli and Pantelides 2017, Tullini and Minghini 2016, Yuan *et al*. 2024), grouted sleeve splices for steel rebars have demonstrated good connection performance, ensuring that the force is transmitted before fracture of the steel bars. The metal sleeve effectively confines the filled cement material, thereby enhancing the bonding characteristics between the steel bars and grout (Ling *et al*. 2016, Hosseini *et al*. 2015, Wang *et al*. 2022). To further improve the splicing behavior of grouted sleeves, researchers have attempted to optimize the geometric shape, processing technology, sleeve material, and other sleeve parameters. Numerous commercial and proprietary products are now available, such as Lenton Interlok, NMB Splice Sleeve, and TTK Tops-joint (Zheng *et al*. 2018). However, the high expense of patented grouted sleeves has obstructed their wide application in prefabricated concrete structures. Einea *et al*. (1995) fabricated a nonproprietary sleeve from a normal steel tube, which is inexpensive but delivers good connection behavior. However, steel tubes commonly have a smooth interior surface that weakens the bonding strength

*Corresponding author, Ph.D.,
E-mail: lihuawei3880@126.com

http://www.techno-press.org/?journal=acc&subpage=7 ISSN: 2287-5301 (Print), 2287-531X (Online)

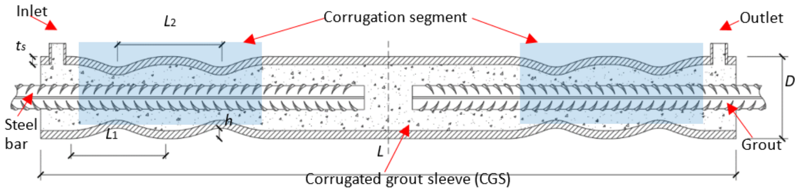

Fig. 1 Geometric configuration of the CGS

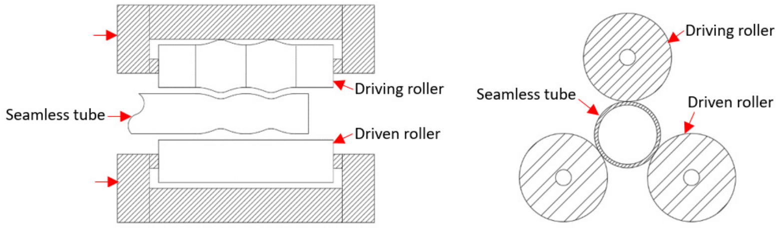

Fig. 2 Schematic of the rolling processing method

between the sleeve and the grouted material. To solve this problem, subsequent researchers proposed nonproprietary grouted sleeves with various configurations such as wedges (Lu *et al*. 2019), threads (Henin and Morcous 2015), rolling pipes (Zheng *et al*. 2018), surface forming (Gao and Zhao 2022), bolts (Sayadi *et al*. 2014), and welded bars and tapered heads (Ling *et al*. 2016). Uniaxail loading tests clarified that increasing the bonding behavior between the grout material and sleeve improves the connection performance, but the above improvement measures are usually complicated and difficult to scale up. Moreover, the connection behavior of grout sleeves fabricated from ordinary steel tubes under cyclic loading is largely unknown. To simplify the machining process and reduce the cost, the present paper develops a new connection technology for steel bars called the corrugated grouted sleeve (CGS) splice (see Fig. 1), which is manufactured by rolling an ordinary seamless steel tube as shown in Fig. 2. The corrugation segment is deemed essential for enhancing the grout confinement and improving the bonding strength at the grout/sleeve interface. Rolling technology enables low-budget fabrication of the CGS. The merits of the CGS are itemized below.

(1) The ordinary seamless steel tube is relatively cheap and the manufacturing process of CGS is obviously simple. Therefore, the proposed sleeve can be fabricated at very low cost.
(2) After rolling, the smooth interior surface of the CGS facilitates the material bonding under cyclic loading, avoiding the stress concentration that typically occurs in traditional ribbed sleeves.
(3) The grooves in the sleeve trigger wedge actions that increase the confinement of the bonding material and prevent interfacial slippage between grout and sleeve. Therefore, the splicing performance is greatly improved.

In the present paper, CGSs for splicing steel rebars are experimentally investigated under cyclic loading. The primary purposes of the research are as follows: (a) to evaluate the splicing characteristics of CGSs for steel rebars under cyclic loading; (b) to examine the effects of steel-bar diameter and loading protocol on the connection behavior of the CGS; and (c) to analyze the wedge action provided by the corrugation and account for the wedge action in a method that captures the confinement stress of the CGS splicing for steel rebars.

2. Experimental program

The CGS specimens were produced by rolling an ordinary seamless steel tube. To evaluate the cyclic performance of the CGS for connecting steel bars, 18 specimens were manufactured and tested under cyclic loading wth large displacement and large stress. The specimens are described in Table 1. The specimens are named by their test mode and steel-bar diameter: “T,” “DC,” and “SC” denote specimens tested under axial tension load, cyclic loading at large displacement, and cyclic loading under large stress, respectively. The digits “16” and “20” refer to steel-bar diameters of 16 and 20 mm, respectively. Three specimens were fabricated in each group to remove the influence of contingency in the tests. A previous study (Wei *et al*. 2023) suggested that two or more grooves provide sufficient anchorage strength for splicing steel rebars. Therefore, two grooves were designed in each half of the sleeve in the present test. The amplitude of the corrugation is another important parameter that greatly affects the connection behavior of CGS. According to previous test results (Wei *et al*. 2023), the corrugation amplitude should exceed 2 mm. Consequently, the groove depths of the CGSs with 16- and 20-mm-diameter steel rebars were 4.5 and 5 mm, respectively. The production process of the specimens is illustrated in Fig. 3. Using iron wire, four CGSs were first attached to each surface of sticks with square cross sections (Fig. 3(b)). Next, two steel rebars were embedded and centered in the CGSs. To prevent overflow of the grout material, a rubber plug was placed at both ends of each CGS. Finally, the square sticks attached

Table 1 Details of the specimens

Specimens	Number	Rebar diameter (mm)	Dimension of CGS (mm)			h	L_1	L_2	n
			L	t_s	D				
T16	1	16	310	4	45	4.5	40	45	2
	2	16	310	4	45	4.5	40	45	2
	3	16	310	4	45	4.5	40	45	2
DC16	1	16	310	4	45	4.5	40	45	2
	2	16	310	4	45	4.5	40	45	2
	3	16	310	4	45	4.5	40	45	2
SC16	1	16	310	4	45	4.5	40	45	2
	2	16	310	4	45	4.5	40	45	2
	3	16	310	4	45	4.5	40	45	2
T20	1	20	370	5	52	5	43	49	2
	2	20	370	5	52	5	43	49	2
	3	20	370	5	52	5	43	49	2
DC20	1	20	370	5	52	5	43	49	2
	2	20	370	5	52	5	43	49	2
	3	20	370	5	52	5	43	49	2
SC20	1	20	370	5	52	5	43	49	2
	2	20	370	5	52	5	43	49	2
	3	20	370	5	52	5	43	49	2

*Note: L = length of CGS; D = outer diameter of steel pipe; t = thickness of steel pipe; h = depth of grooves; L_1 = length of corrugation; L_2 = gap between adjacent corrugations; n = number of corrugations

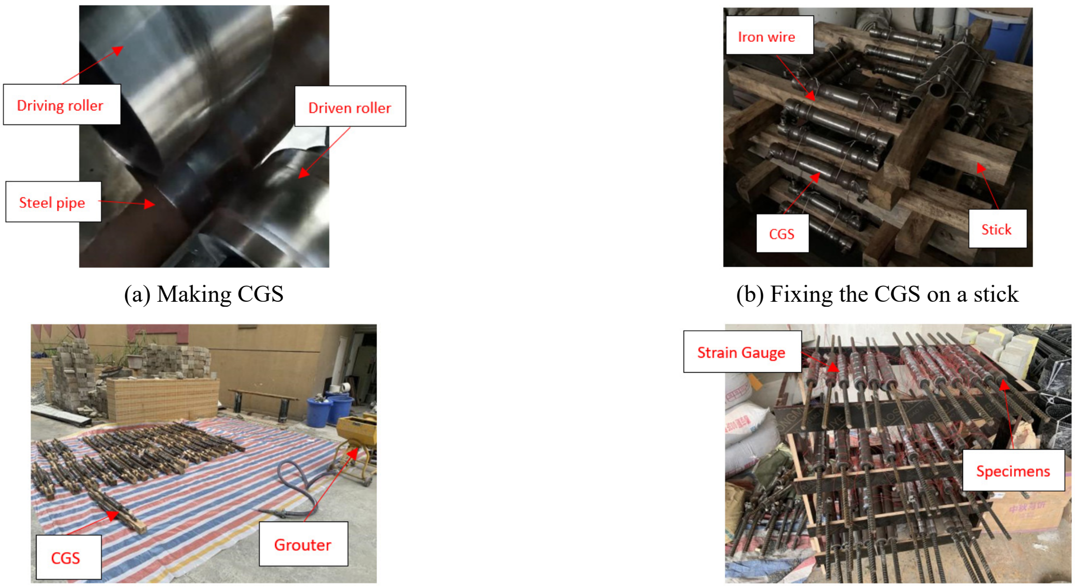

(a) Making CGS

(b) Fixing the CGS on a stick

(c) Injecting the grout material

(d) Finishing the splicing bars by CGS

Fig. 3 Fabrication process of the test specimens

with their specimens were upended and the grout was filled into the sleeve through a grout pump at the inlet. When the grout overflowed from the outlet, the pump was shut and the sleeve was considered to be filled with grout. The specimens were cured for 28 days prior to testing.

The test CGSs for splicing HPB400E steel rebars were manufactured from 45# seamless steel tubes with different diameters (45 and 52 mm for rebar diameters of 16 and 20 mm respectively). The material properties of the steel rebars are summarized in Table 2. Low-shrinkage grout was utilized as the bonding material in the connection. Through standard material tests, the average compressive strength was determined as 98.87 MPa. The cyclic load during the tests was provided by an electro-hydraulic-servo material

Table 2 Material properties of the rebars

Nominal diameter (mm)	$f_{sy,r}$ (MPa)	$f_{su,r}$ (MPa)	$A_{e,r}$ (%)	E_r (MPa)
16	446	530	31	2.0×10^5
20	424	533	35	2.0×10^5

*Note: $f_{sy,r}$ = Yield stress of rebar; $f_{su,r}$ = ultimate stress of rebar; E_r = elastic modulus of rebar; $A_{e,r}$ = elongation of rebar

testing machine. The test setup is shown in Fig. 4. According to the JGJ 107 standard (JGJ 107-2016 2016), high-stress cyclic loading is governed by force. The applied tension load was $0.9f_{ys}$, where f_{ys} is the yield strength of the steel rebar, then unloaded to $0.5f_{ys}$, and finally restored to $0.9\ f_{ys}$. This loading cyclic was applied 20 times. After cyclic loading tests, the specimens were pulled until they failed. Under cyclic loading with large displacement, the loading protocol is controlled by force and displacement.

The strain evolution of each GCS was measured by 22 electrical resistance strain gauges mounted on the specimen as shown in Fig. 6. Meanwhile, to measure the residual deformation, the specimens were mounted on an extensometer clamped on fixtures as shown in Fig. 7.

3. Results and discussion

3.1 Failure modes

The failure modes of all specimens were steel-bar ruptures, which are preferred over steel-bar pullout or sleeve failure (see Fig. 8) because they indicate sufficient anchoring strength of the splicing steel bars in the proposed connection system. That is, force can be effectively transferred among the precast concrete components. Prior to steel-bar yield, no obvious phenomenon were observed in the specimens and the working condition of the CGS splices was high. The grooves in the CGS improved the bonding strength at the sleeve/grout and grout/bar interfaces,

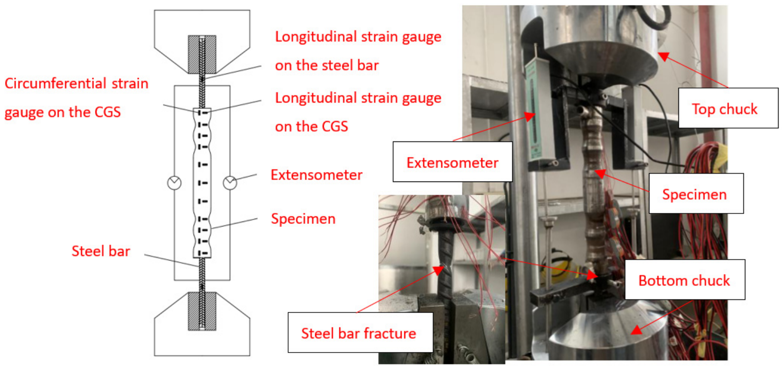

Fig. 4 Test setup

(a) Under large stress (b) Under large displacement

Fig. 5 Loading protocol of the test specimens

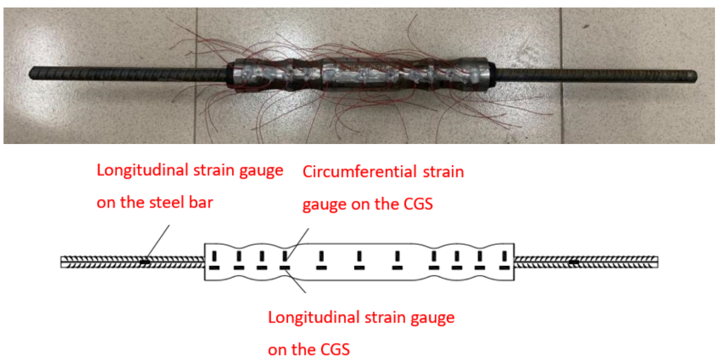

Fig. 6 Schematic of the attachment positions of the strain gauges

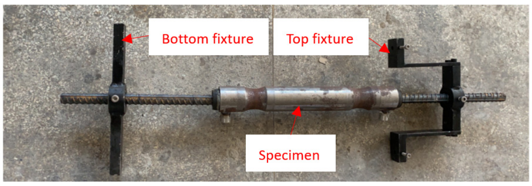

Fig. 7 Fixing equipment for the extensometer

facilitating the delivery of tension force from the steel bars. When the load reached approximately $5\varepsilon_{ys}$, grout splitting at the CGS ends was clearly audible. As the load further increased, cracks continuously developed in the bonding material at both ends of the sleeve. Slight peeling of the grout was observed until the steel bar ruptured.

To further investigate the connection performance of the CGS splicing under cyclic loading, the specimens were longitudinally cut into two halves by a water-jet cutting machine. The grout confined by the CGS was robustly anchored to the steel bars (Fig. 9) and no obvious cracks appeared in the middle part. Moreover, no slippage occurred at the sleeve/grout and grout/bar interfaces.

2.2 Assessment of connection performance

The JGJ 107-2016 standard (JGJ 107-2016 2016) specifies three grades of grout sleeve splices with different requirements (see Table 3). The tension strengths of all specimens were $1.10f_{uss}$ or higher, as recommended in the Chinese design code. Here, f_{uss} refers to the standard tension

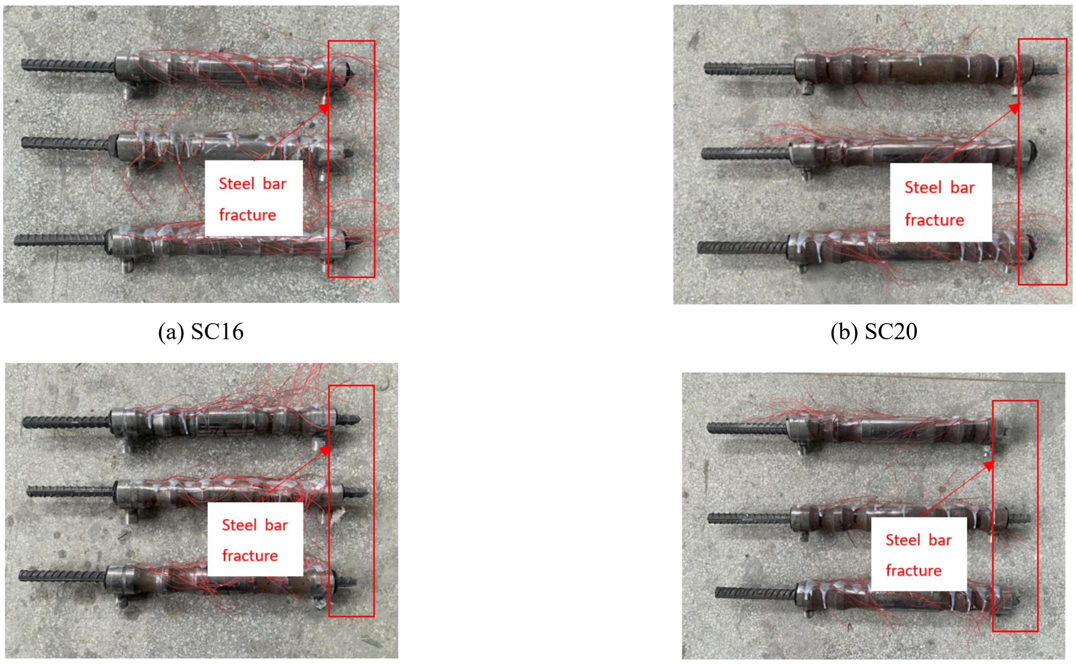

(a) SC16 (b) SC20

(c) DC16 (d) DC20

Fig. 8 Failure modes of the CGS splices under cyclic loading

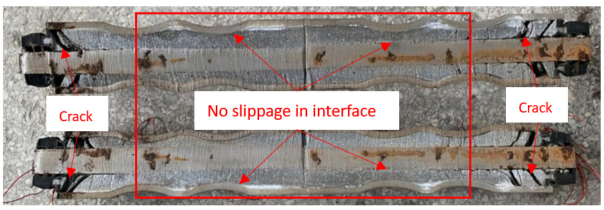

(a) Longitudinal cross sections of a specimen subjected to large stress

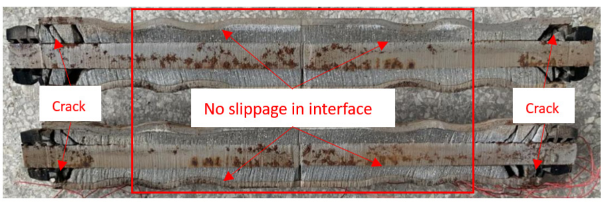

(b) Longitudinal cross-sections of a specimen subjected to large displacement

Fig. 9 Interior views of CGS splices after cyclic loading

Table 3 Classification of joints based on deformation

Grade of joint		I class	II class	III class
Cyclic loading at large stress	Residual deformation (mm)	$u_{20} \leq 0.3$	$u_{20} \leq 0.3$	$u_{20} \leq 0.3$
Cyclic loading at large displacement		$u_4 \leq 0.3$ and $u_8 \leq 0.6$	$u_4 \leq 0.3$ and $u_8 \leq 0.6$	$u_8 \leq 0.6$

*Note: u_{20} = Residual deformation after 20 cyclic loads at large stress; u_4 = residual deformation after 4 cyclic loads at large displacement; u_8 = residual deformation after 8 cyclic loads at large displacement

Table 4 Test results of the CGSs for splicing rebars under a uniaxial tension load

Specimen	Specimen number	P_y (kN)	P_u (kN)	R_y	R_s	R_d	u_4 (mm)	u_8 (mm)	U_{20} (mm)	Failure mode
T16	1	99.61	126.21	1.24	1.57	10.77				Rebar fracture
	2	101.32	127.50	1.26	1.59	8.31				
	3	100.21	126.01	1.25	1.57	15.07				
SC16	1	98.21	124.50	1.22	1.55	9.08			0.15	
	2	99.58	125.12	1.24	1.56	11.28			0.14	
	3	99.12	124.15	1.23	1.54	10.39			0.15	
DC16	1	96.38	124.65	1.20	1.55	12.58	0.15	0.34		
	2	98.94	125.04	1.23	1.56	10.43	0.17	0.35		
	3	98.59	124.74	1.23	1.55	11.07	0.16	0.35		
T20	1	148.21	197.10	1.18	1.57	9.90				
	2	147.85	196.05	1.18	1.56	12.04				
	3	151.09	197.95	1.20	1.58	8.40				
SC20	1	148.56	196.17	1.18	1.56	8.97			0.16	
	2	147.79	194.21	1.18	1.55	12.42			0.15	
	3	146.72	195.12	1.17	1.55	10.81			0.17	
DC20	1	149.28	195.38	1.19	1.56	9.17	0.19	0.37		
	2	148.71	196.26	1.18	1.56	12.09	0.18	0.37		
	3	148.53	196.32	1.18	1.56	10.48	0.18	0.38		

*Note: P_y = Yield load of CGS splice; P_u = ultimate load of CGS splice

strength of an HRB400 steel bar. After 20 high-strength cycles (where the maximum stress reached $0.9f_{ys}$), the residual deformation u_{20} of the CGS connection was measured as 0.14–0.17 mm (i.e., below 0.3 mm). Under the high-strain cyclic tests, the residual deformations u_4 and u_8 were obtained as 0.15–0.18 mm and 0.34–0.38 mm, respectively, where u_4 and u_8 are the residual deformations after the first four cycles at $2\varepsilon_{ys}$ to $-0.5f_y$ and the second four cycles at $2\varepsilon_{ys}$ to $-0.5f_y$, respectively. The u_4 and u_8 were less than 0.3 mm and 0.6 mm, respectively, indicating that the proposed CGS splice for steel bars is a first-grade joint in the JGF 107-2016 standard.

As suggested by Ling (Ling *et al*. 2016), the connection properties of the CGS splices for steel bars were further characterized by their strength ratio R_s, yield ratio R_y, and ductility ratio R_d, which are respectively calculated as follows

$$R_y = \frac{f_{yc}}{f_{ys}} \tag{1}$$

$$R_s = \frac{f_{uc}}{f_{ys}} \tag{2}$$

$$R_d = \frac{u_{uc}}{u_{yc}} \tag{3}$$

where f_{yc} and f_{uc} are the yield and ultimate stress of the CGS splice, respectively, f_{ys} is the specified yield stress of the steel bar, and u_{yc} and u_{uc} are the corresponding displacements at yield and failure of the specimen, respectively.

The test results are listed in Table 4. According to the JGJ 107-2016 and ACI 318-11 standards, R_y should exceed 1.0, R_s should not be less than 1.25, and R_d should exceed 4.0. As seen in Table 4, all specimens satisfied the limits on yield ratio, strength ratio, and ductility ratio specified in the design codes. These results confirm the good splicing performance of the CGS system. In particular, the creative corrugated configuration resisted cyclic loading of the connecting steel bars.

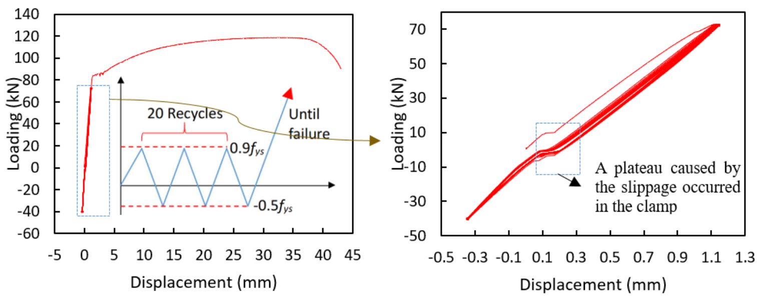

(a) SC16-1

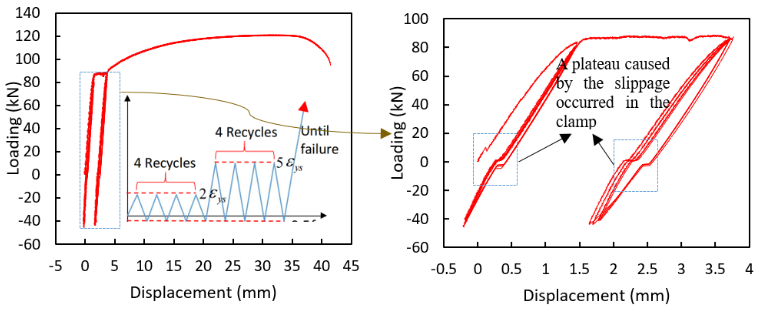

(b) DC16-1

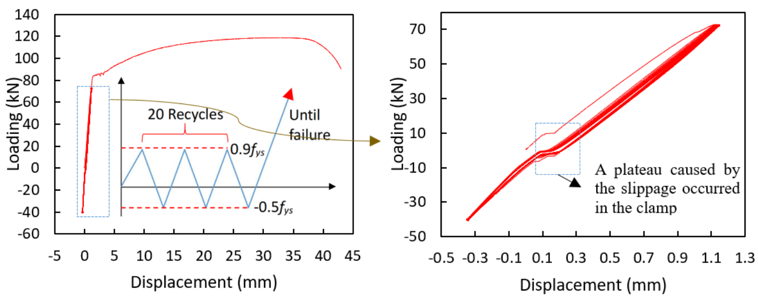

(c) SC20-1

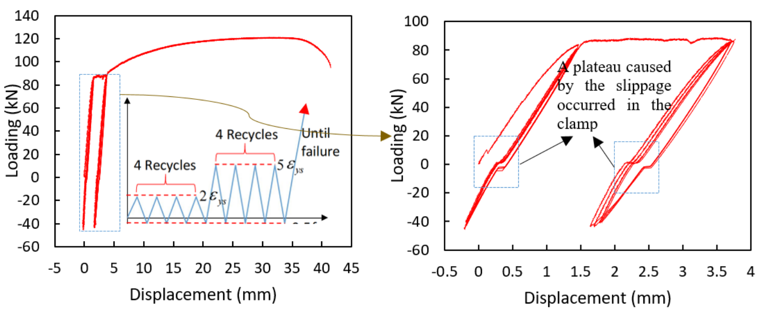

(d) DC20-1

Fig. 10 Typical load–displacement plots of the specimens under different loading conditions

2.3 Relationship between load and displacement

Fig. 10 plots the load–displacement relationships of the CGS splices under cyclic loading. The plots obtained under high-stress cyclic loading are almost linear and the loading and unloading paths nearly overlap (Fig. 10(a)). As the cyclic test was performed in the elastic region, the cyclic loops open only slightly and enclose a small area, indicating low energy consumption. The curves are considered to be smooth with no sharp changes except at the moment of switching the loading direction. The plateau near the origin is mainly caused by slippage in the clamp. Meanwhile, under large-displacement cyclic loading, the looped curves are linear and similar during the first cyclic level but the area enclosed by the curves increases after the second cyclic level, probably because the second-stage cyclic behavior was influenced by interface damage accumulated during the first cyclic test. Moreover, a small break is visible near the coordinate point at which the loading direction changed. The connection performance is considered to be stable without saltation. Finally, the residual deformation meets the requirements of the design codes.

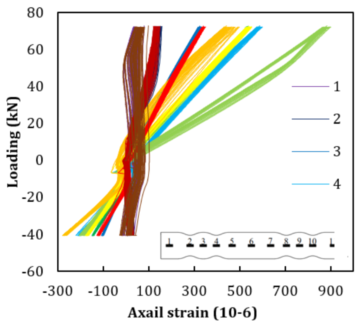

(a) Axial strain of SC16

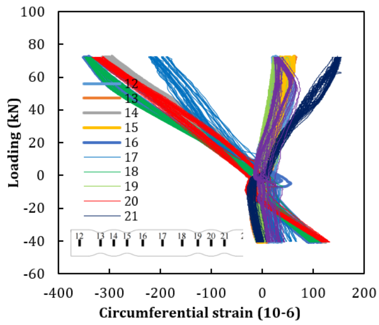

(b) Circumferential strain of SC16

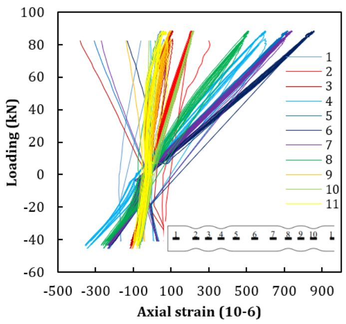

(c) Axial strain of DC16

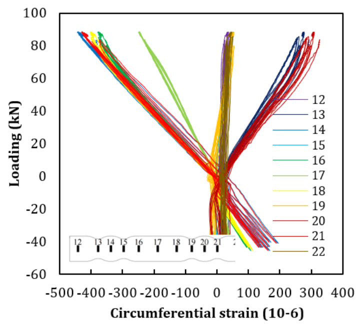

(d) Circumferential strain of DC16

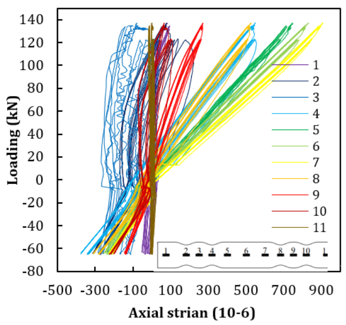

(e) Axial strain of SC20

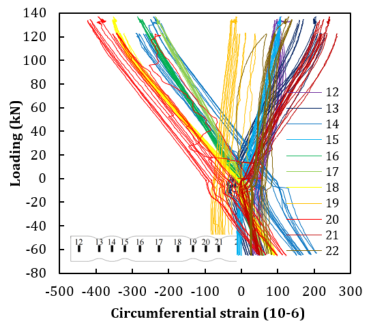

(f) Circumferential strain of SC20

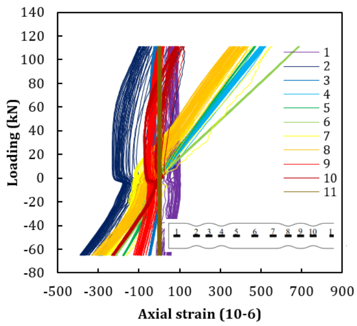

(g) Axial strain of DC20

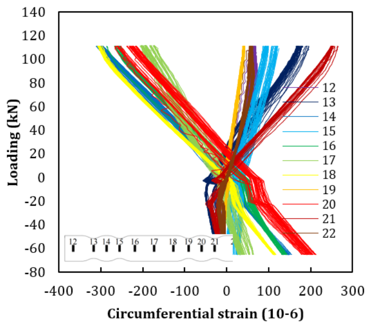

(h) Circumferential strain of DC20

Fig. 11 Strain development plots of the CGSs under cyclic loading

2.4 Strain evolution of the CGSs

Fig. 11 shows the strain development of the CGSs under cyclic loading. The curves exhibit an almost elastic response. In these tests, the tension load was defined as positive and the compressive load was considered to be negative. The curves nearly overlap at negative vertical coordinates, preventing a clear discussion of the results.

Therefore, only the relationship between tension loading and strain is discussed here. The longitudinal strain is positive like the tension-loading direction. In the circumferential direction, the strain should be negative owing to the Poisson effect. However, positive strain values were recorded in the groove because the groove section expands. Such expansion is usually triggered by the bonding material. The tension loading acting on the steel bars is transmitted to the grout through the grout/bar interface, so the groove mainly resists the force from the bonding material. Clearly, the groove in the sleeve plays a crucial role in the splicing behavior.

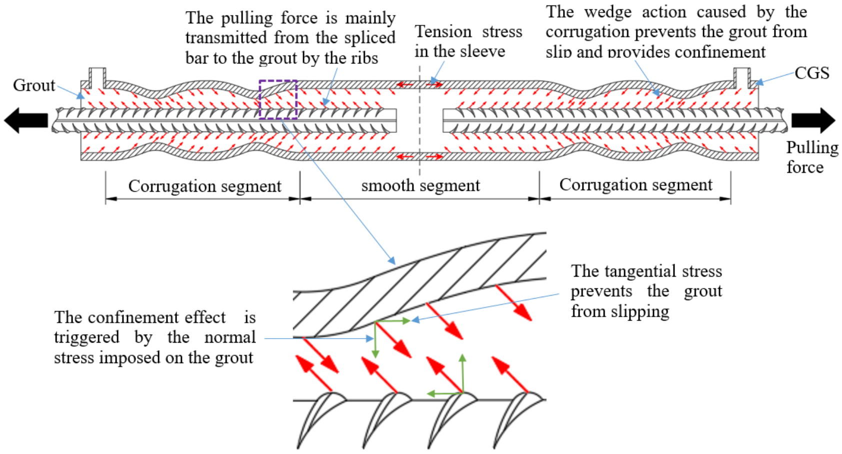

Fig. 12 Schematic of the force transmission process in the CGS connection

4. Discussion of test results

4.1 Mechanical mechanism of the CGS connection

Fig. 12 is a schematic of the force transmission process in the CGS splice. The bond strength at the grout/bar interface is generally governed by interlocking action of the ribs on the bar. The sleeve is separated into two parts: a smooth segment and a corrugation segment. In the smooth segment, the force from the steel bars is delivered to the metal pipe through the sleeve/grout interface. Friction and chemical adhesion play key roles in this process. The circumferential compressive stress in the sleeve wall is mainly caused by the Poisson effect. Although the interlocking action at the grout/bar interface tends to split and expand the grout, the hoop tension stress exerted by grout expansion in the transverse section of the sleeve is relatively small. Because the grout-confinement effect is weak in the smooth part of the CGS, the stress in this part is compressive, as recorded by the gauges during the test.

Meanwhile, the grooves in the corrugation segment considerably affect the interface behavior (see Fig. 12). In particular, they increase the interaction force between the grout and CGS. The interaction stress can be divided into normal and longitudinal stresses. The longitudinal stress prevents slippage at the sleeve/grout interface while the normal stress enhances the confinement action on the grout. The same findings are reported elsewhere (Harajli 2009, Bournas and Triantafillou 2011, Afefy and El-Tony 2016, Sayadi *et al*. 2014). The radial stress caused by the normal stress on the grout effectively resists the evolution of splitting cracks triggered by the interlocking action between the steel bar and bonding material. Therefore, it was considered that the grooves on the sleeve improved the confinement effect of the CGS on the grout material, thereby enhancing the bond strength at the grout/bar interface.

4.2 Analytical model

The bonding force P_s between the grout and sleeve in the smooth part of the GCS is calculated as

$$P_s = (\varepsilon_m - \varepsilon_s)E_s A_s \tag{4}$$

where ε_m is the measured longitudinal strain in the middle of the sleeve, ε_s is the strain recorded by the gauge along the axial direction of the smooth segment, E_s is the modulus of elasticity of the seamless steel pipe, and A_s is the cross-sectional area of the sleeve. The bonding force P_c at the grout/sleeve interface in the corrugation part is then given by

$$P_c = P_u - P_s \tag{5}$$

where P_u is the ultimate load of the connection. As listed in Table 5, the smooth part provides approximately 35%–60% of the bonding force depending on the rebar diameter (16 or 20 mm). That is, the wedge action in the corrugation segment does not fully develop and the bonding-strength contribution of the grooves increases with rebar diameter.

The bonding force P_c at the grout/sleeve interface is mainly contributed by the friction force P_f and mechanical interlock P_{mx} between the grout and grooves, both acting in the corrugation portion. Therefore, it is expressed as

$$P_c = P_f + P_{mx} \tag{6}$$

in which P_f and P_{mx} are respectively determined as

$$P_f = \mu p_{my} \pi (d_s - h) n L_1 \tag{7}$$

$$P_{mx} = p_{mx} \pi (d_s - h) n L_1 \tag{8}$$

where p_{mx} and p_{my} are the average tangential and normal stresses on the groove in the corrugation part, respectively, d_s is the inner diameter of the sleeve, h, n, and L_1 are the depth, number, and width of the grooves, respectively, and μ is the friction coefficient. As the grooves are inclined by approximately 45°, we can write

$$p_{mx} = p_{my} \tag{9}$$

Combining Eqs. (4)-(9), the average groove-triggered confinement stress p_{my} on the grout in the corrugation segment can be written as

Table 5 Contributions of bond force in the corrugation and smooth segments

Specimen	τ_s (MPa)	P_s (kN)	τ_c (MPa)	P_c (kN)	P_c/P_u (%)
T16	9.88	45.93	8.16	80.64	64
SC16	9.42	43.78	8.32	82.25	65
DC16	10.55	49.04	7.78	76.82	61
T20	15.04	110.15	12.05	86.88	44
SC20	15.63	114.49	11.26	81.18	41
DC20	14.71	107.71	12.09	87.10	45

$$p_{my} = \frac{P_u - (\varepsilon_m - \varepsilon_s)E_s A_s}{\pi n(d_s - h)(\mu + 1)L_1} \tag{10}$$

In the smooth segment, the static equilibrium equation (see Fig. 14) is given by

$$2F = p_s d_s L_s \tag{11}$$

where F is the tensile force in the transverse section of the sleeve, p_s is the average confinement stress on the grout in the smooth part, and L_s is the length of the smooth segment. As the sleeves remain in the elastic region during the test, the tensile force F is also expressed as

$$F = E_s \varepsilon_{cs} t_s L_s \tag{12}$$

where the transverse strain ε_{cs} on the sleeve can be measured by the circumferential gauges, and t_s is the thickness of the seamless steel pipe.

Substituting Eq. (12) into Eq. (11), the confinement stress on the grout is determined by

$$p_s = \frac{2E_s \varepsilon_{cs} t_s}{d_s} \tag{13}$$

Table 6 gives the confinement stresses calculated by Eqs. (10) and (13). The confinement stress in the smooth part is approximately 36%-42% that in the corrugation segment of the specimens with 16-mm-diameter connecting steel bars, rising to 41%-45% in the specimens with 20-mm-diameter connecting steel bars. The grooves notably enhance the confinement effect on the grout, thereby increasing the bonding properties at the grout/bar interface. This result also agrees with the test results.

Table 6 Calculated confinement stresses in the corrugation and smooth segments

Specimen	T16	SC16	DC16	T20	SC20	DC20
p_{my} (Mpa)	10.29	10.17	11.03	12.57	12.31	12.85
p_s (Mpa)	4.35	4.12	4.01	5.18	5.34	5.78
p_s/p_{my} (%)	42.27	40.51	36.35	41.21	43.38	44.98

5. Conclusions

To improve the splicing behavior of steel bars in precast structures, this paper developed a novel and low-cost corrugated grouted sleeve (CGS) by rolling a seamless pipe. Eighteen specimens fabricated from 45# seamless pipe with various parameters were prepared and tested under cyclic loading. The connection characteristics of splicing steel bars in prefabricated structures provide lateral load resistance. The main conclusions drawn from the study are summarized below.

(1) The proposed connection system provides sufficient anchoring strength of the splicing steel bars, enabling effective force transfer between precast concrete components. All specimens satisfied the yield ratio, strength ratio, and ductility ratio stipulated in code standards, proving that the CGS system has good splicing performance and provides cyclic-loading resistance to the connecting steel bars. This performance is enabled by the creative corrugated configuration.

(2) The longitudinal stress prevents slippage at the sleeve/grout interface while the normal stress enhances the confinement action on the grout. Therefore, the grooves on the sleeve are thought to enhance the confinement effect of CGS on the grout material, thereby enhancing the bond strength at the grout/bar interface.

(3) A model that calculates the confinement stresses in the corrugation and smooth segments was proposed. The confinement stress in the smooth part of each specimen is approximately 36%–45% that in the corrugation segment, depending on the diameter of the steel bars (16 or 20 mm). This result consolidates the test results, clarifying that grooves enhance the confinement effect on the grout, thereby increasing the bonding properties at the grout/bar interface.

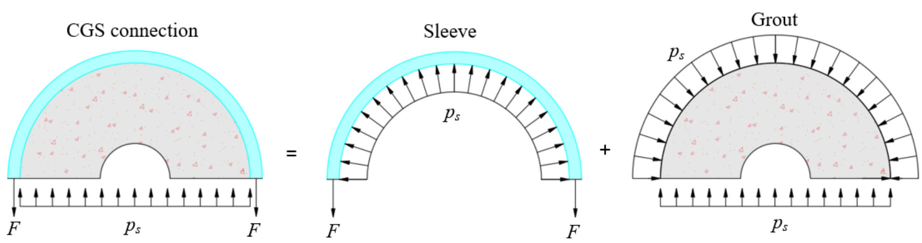

Fig. 14 CGS connection in the transverse section at equilibrium

Acknowledgments

The authors gratefully acknowledge the financial support provided by the Natural Science Foundation of Fujian Province (2022J011195), Resource chemical industry and technology Foundation of Nanping (N2021Z002), Undergraduate innovation and entrepreneurship project (202410397015).

References

ACI Committee 439 (1999), Mechanical Connections of Reinforcing Bars, American Concrete Institute, Farmington Hills, MI, USA.

Afefy, H.M. and El-Tony, E.T.M. (2016), "Bond behavior of embedded reinforcing steel bars for varying levels of transversal pressure", *J. Perform. Constr. Facil.*, **30**(2), 04015023. https://doi.org/10.1061/(ASCE)CF.1943-5509.0000768

Al-Azzawi, A.A., Daud, R.A. and Daud, S.A. (2020), "Behavior of tension lap spliced sustainable concrete flexural members", *Adv. Concrete Constr., Int. J.*, **9**(1), 83-92. https://doi.org/10.12989/acc.2020.9.1.083

Alias, A., Sapawi, F., Kusbiantoro, A., Zubir, M.A. and Abd Rahman, A.B. (2014), "Performance of grouted splice sleeve connector under tensile load", *J. Mech. Eng. Sci.*, **7**, 1094-1102. https://doi.org/10.15282/jmes.7.2014.8.0106

Ameli, M.J. and Pantelides, C.P. (2017), "Seismic analysis of precast concrete bridge columns connected with grouted splice sleeve connectors", *J. Struct. Eng.*, **143**(2), 1-13. https://doi.org/10.1061/(ASCE)ST.1943-541X.0001678

Bournas, D.A. and Triantafillou, T.C. (2011), "Bond strength of lap-spliced bars in concrete confined with composite jackets", *J. Compos. Constr.*, **15**(2), 156-167. https://doi.org/10.1061/(ASCE)CC.1943-5614.0000078

Einea, A., Yamane, T. and Tadros, M.K. (1995), "Grout-filled pipe splices for precast concrete construction", *PCI J.*, **40**(1), 82-93. http://worldcat.org/oclc/12789822

Elliott, K.S. (2017), *Precast Concrete Structures*, Taylor & Francis Group, CRC press, Boca Raton, FL, USA.

Gao, Q. and Zhao, W.J. (2022), "Experimental study on performance of grouted sleeve connection with surfacing forming under uniaxial tensile load", *J. Build. Struct.*, **43**(4), 208-219. https://doi.org/10.14006/j.jzjgxb.2020.0329

Haber, Z.B., Saiidi, M.S. and Sanders, D.H. (2014), "Seismic performance of precast columns with mechanically spliced column-footing connections", *ACI Struct. J.*, **111**(3), 639-650. https://doi.org/10.14359/51686624

Harajli, M.H. (2009), "Bond stress–slip model for steel bars in unconfined or steel, FRC, or FRP confined concrete under cyclic loading", *J. Struct. Eng.*, **135**(5), 509-518. https://doi.org/10.1061/(ASCE)0733-9445(2009)135:5(509)

He, A., Zheng, D.C., Cai, J., Chen, Q.J., Tang, X.L. and Ye, J.B. (2024), "Experimental investigation on the horizontal impact response of precast RC bridge piers with grouted sleeve connections considering defects", *Eng. Struct.*, **316**, 118617. https://doi.org/10.1016/j.engstruct.2024.118617

Hemamalini, S. and Vidjeapriya, R. (2020), "Influence of connection detailing on the performance of wall-to-wall vertical connections under cyclic loading", *Adv. Concrete Constr., Int. J.*, **9**(5), 437-448. https://doi.org/10.12989/acc.2020.9.5.437

Henin, E. and Morcous, G. (2015), "Non-proprietary bar splice sleeve for precast concrete construction", *Eng. Struct.*, **83**, 154-162. https://doi.org/10.1016/j.engstruct.2014.10.045

Hosseini, S.J.A., Rahman, A.B.A., Osman, M.H., Saim, A. and Adnan, A. (2015), "Bond behavior of spirally confined splice of deformed bars in grout", *Constr. Build. Mater.*, **80**, 180-194. https://doi.org/10.1016/j.conbuildmat.2014.12.097

JGJ 107-2016 (2016), Technical Specification for Mechanical Splicing of Steel Reinforcing Bars, China Building Industry Press, Beijing, China.

Joshi, D.D., Patel, P.V., Rangwala, H.M. and Patoliya, B.G. (2020), "Experimental and numerical studies of precast connection under progressive collapse scenario", *Adv. Concrete Constr., Int. J.*, **9**(3), 235-248. https://doi.org/10.12989/acc.2020.9.3.235

Kalogeropoulos, G.I., Tsonos, A.D.G. and Konstantinidis, D. (2019), "Seismic behaviour of RC columns with welded rebars or mechanical splices of reinforcement", *Earthq. Struct., Int. J.*, **17**(3), 297-306. https://doi.org/10.12989/eas.2019.17.3.297

Kuang, Z. and Zheng, G. (2018), "Computational and experimental mechanical modelling of a composite grouted splice sleeve connector system", *Materials*, **11**(2), 306. https://doi.org/10.3390/ma11020306

Kurama, Y.C., Sritharan, S., Fleischman, R.B., Restrepo, J.I., Henry, R.S., Cleland, N.M., Ghosh, S.K. and Bonelli, P. (2018), "Seismic-resistant precast concrete structures: State of the art", *J. Struct. Eng.*, **144**(4), 03118001. https://doi.org/10.1061/(ASCE)ST.1943-541X.0001972

Lee, S.J., Lee, D.H., Kim, K.S., Oh, J.Y., Park, M.K. and Yang, I.S. (2013), "Seismic performances of RC columns reinforced with screw ribbed reinforcements connected by mechanical splice", *Comput. Concrete, Int. J.*, **12**(2), 131-149. https://doi.org/10.12989/cac.2013.12.2.131

Lei, S., Liu, L.J., Wu, F.W., Lin, W.W., Peng, K. and Cao, J.C. (2023), "Seismic performance of short precast columns with UHPC grouted sleeve connections: An experimental and numerical study", *Structures*, **55**, 427-440. https://doi.org/10.1016/j.istruc.2023.06.029

Ling, J.H., Rahman, A.B.A., Ibrahim, I.S. and Hamid, Z.A. (2016), "Tensile capacity of grouted splice sleeves", *Eng. Struct.*, **111**, 285-296. https://doi.org/10.1016/j.engstruct.2015.12.023

Lu, Z., Huang, J., Li, Y., Dai, S., Peng, Z., Liu, X. and Zhang, M. (2019), "Mechanical behaviour of grouted sleeve splice under uniaxial tensile loading", *Eng. Struct.*, **186**, 421-435. https://doi.org/10.1016/j.engstruct.2019.02.033

Parastesh, H., Hajirasouliha, I. and Ramezani, R. (2014), "A new ductile moment-resisting connection for precast concrete frames in seismic regions: an experimental investigation", *Eng. Struct.*, **70**, 144-157. https://doi.org/10.1016/j.engstruct.2014.04.001

Sayadi, A.A., Rahman, A.B.A., Jumaat, M.Z.B., Alengaram, U.J. and Ahmad, S. (2014), "The relationship between interlocking mechanism and bond strength in elastic and inelastic segment of splice sleeve", *Constr. Build. Mater.*, **55**, 227-237. https://doi.org/10.1016/j.conbuildmat.2014.01.020

Sharbatdar, M.K., Jafari, O.M. and Karimi, M.S. (2018), "Experimental evaluation of splicing of longitudinal bars with forging welding in flexural reinforced concrete beams", *Adv. Concrete Constr., Int. J.*, **6**(5), 509-525. https://doi.org/10.12989/acc.2018.6.5.509

Tullini, N. and Minghini, F. (2016), "Grouted sleeve connections used in precast reinforced concrete construction-experimental investigation of a column-to-column joint", *Eng. Struct.*, **127**, 784-803. https://doi.org/10.1016/j.engstruct.2016.09.021

Wang, T., Zhou, Z.J., Yuan, K., Jiang, R.N., Ma, X.Q. and Li, L.W. (2022), "Evaluation of common defects of grouted sleeve connectors", *Case Stud. Constr. Mater.*, **17**, e01605. https://doi.org/10.1016/j.cscm.2022.e01605

Wei, M.W., Du, J.R., Li, H.W., Lei, N.Z., Huang, Y.Y. and Xiao, B.R. (2023), "Behavior of a novel corrugated grouted sleeve splice for prefabricated construction under uniaxial tensile loading", *Adv. Struct. Eng.*, **26**(7), 1353-1374.

https://doi.org/10.1177/13694332231161099

Xiao, J.Z., Liu, L.L., Ding, T. and Xie Q.H. (2020), "Experimental study on mechanical behavior of thermally damaged grouted sleeve splice under cyclic loading", *Struct. Concrete*, **21**(6), 2494-2514. https://doi.org/10.1002/suco.202000092

Yuan, W.T., Wang, Y.R., Dong, Z.X. and Fang, Q.H. (2024), "Experimental study on mechanical properties of corroded grouted sleeve splice", *Constr. Build. Mater.*, **412**, 134797. https://doi.org/10.1016/j.conbuildmat.2023.134797

Zheng, Y.F., Guo, Z.X., Guan, D.Z. and Zhang, X. (2018), "Parametric study on a novel grouted rolling pipe splice for precast concrete construction", *Constr. Build. Mater.*, **166**, 452-463. https://doi.org/10.1016/j.conbuildmat.2018.01.182